Processing and Application of Ceramics 18 [3] (2024) 307–313
https://doi.org/10.2298/PAC2403307L

Comparative assessment of structural, magnetic and impedance properties of xLaMnO$_3$–(1-x)BiFeO$_3$ solid solutions

Aryan Singh Lather[1,*], Shubhpreet Kaur[2,*], Manikant Paswan[3]

[1]*Department of Physics, Guru Jambheshwar University of Science & Technology, Hisar, 125001, Haryana, India*
[2]*Department of Physics and Photonics, National Institute of Technology, Hamirpur, Himachal Pradesh, 177005, India*
[3]*Department of Mechanical Engineering, Sant Longowal Institute of Engineering & Technology, Longowal, Sangrur, 148106, India*

Received 7 May 2024; Received in revised form 31 August 2024; Accepted 15 September 2024

Abstract

BiFeO$_3$ (BFO) is extensively researched due to its lead-free composition, high ordering temperature, remarkable polarization and useful electric and magnetic switching mechanism for data storage devices. On the other hand, the superexchange ordered system of LaMnO$_3$ (LMO) is well-suited for fuel cells. This study examines the structural, magnetic and impedance properties of xLaMnO$_3$–(1-x)BiFeO$_3$ solid solutions (x = 0.05, 0.10 and 0.20) prepared using the solid state reaction method and sintering. X-ray diffraction technique confirmed single phase material with the hexagonal structure and R3c symmetry. The vibrating sample magnetometer showed the change from antiferromagnetic behaviour of BFO to weak ferromagnetic behaviour of BFO/LMO ceramics and maximum remnant magnetization of 0.206 emu/g for x = 0.10. The superexchange interactions are responsible for this magnetic behaviour. Impedance analysis was used to investigate the dielectric relaxation and the negative temperature coefficient of resistance.

Keywords: *BiFeO$_3$, LaMnO$_3$, solid solution, ferromagnetic behaviour, impedance spectroscopy*

I. Introduction

Memory-based data storage systems mostly use electric or magnetic swapping methods. However, the migration of charge carriers induced by the current-induced magnetization flipping mechanism results in Joule heating and higher power consumption. In contrast, the ability to charge or the method used in electric field switching can considerably minimize the loss of energy by a considerable amount [1].

In a perfect world, controlling the electromagnetic field can greatly decrease changing power while enhancing non-volatile performance. Magnetic field-coupled polarization or electric field-coupled magnetization is both possible in multiferroic compounds. These materials can therefore provide low-power, high-density information retention with quick electrical copying and quick magnetic retrieving [2].

BiFeO$_3$ (BFO) has garnered significant attention in research due to its lead-free composition, high Curie temperature and remarkable polarization properties [3]. The general magnetic moment and the magnetoelectric interaction are nevertheless decreased by its antiferromagnetic arrangement with a cycloidal spin structure. Researchers have explored various alternative approaches, including solid solutions, multiphase composites and atomically engineered superlattices comprising ferroic constituents to tackle this challenge. The objective of these strategies is to enhance magnetoelectric performance [4]. In ferroelectric or multiferroic substances, it is feasible to get a better response by using a composition-driven morphotropic phase boundary [5,6]. Ji *et al.* [7] have studied the influence of sintering temperature on microstructure, electrical and magnetic properties of BiFeO$_3$-BaTiO$_3$ solid solution ceramics. Fan *et al.* [8] studied the dielectric relaxation charac-

* Corresponding author: tel: +91 9466962130
e-mail: *shubhpreetbawa@gmail.com* (S. Kaur)
aryansinghlather@gmail.com (A.S. Lather)

teristics of solid solution in $BiFeO_3/BaTiO_3$ system obtained by the microwave sintering method. Similarly, Chen *et al.* [9] reported the dielectric and ferroelectric properties of $BiFeO_3$ modified with $BaTiO_3$-$BiYbO_3$ based solid solution ceramics. Gian *et al.* [10] investigated the effects of $(Bi_{0.5}Li_{0.5})TiO_3$ addition on microstructure, electrical properties and thermal stability of $BiFeO_3$-$BaTiO_3$ piezoelectric ceramics. In addition, Ao *et al.* [11] prepared solid solution with composition $Bi_{0.78}La_{0.08}Sm_{0.14}Fe_{0.85}Ti_{0.15}O_3$ ($BiFeO_3$ co-doped at A and B sites) by solid-state method and confirmed its ferromagnetic behaviour.

By combining polar BFO with superexchange ordered $ReMnO_3$ (Re = Rare earth) in a phase-separated composite, the researcher increased the magnetic moment [12]. The bulk contact between the two antiferromagnetic entities was credited for the increased magnetic moment. This interface theory was supported by spectroscopic methods like neutron diffraction [13]. Rare earth manganites, characterized by their interconnected charge, spin and orbital degrees of freedom, exhibit intriguing phenomena [9]. In a study conducted by Yu *et al.* [14], atomic-scale junctions were employed to demonstrate the suppression of bulk polarization by utilizing ferromagnetic $La_{0.7}Sr_{0.3}MnO_3$ in conjunction with a multiferroic BFO surface. Similar to this, altering the Mn cations in $La_{0.5}Ca_{0.5}MnO_3$ by mechanical bonding can affect the canted moments of BFO [15]. According to the conditions during setup, the manganite species itself exhibit a variety of behaviours. While bulk $La_{0.7}Sr_{0.3}MnO_3$ maintains its rhombohedral structure despite undergoing a metal-insulator change, the same material when present as a nanomaterial goes through this transition and develops an orthorhombic pattern [16,17]. This nanomaterial system offers a promising matrix for increasing the multiferroic characteristics of BFO. This is evident through its structured magnetic core, disordered shell and elevated electrical resistance. Although there are several researchers who have been studying the BFO/LMO system, their structure, magnetic and impedance properties have not been explored in deep. Thus, the basic and preliminary studies of BFO/LMO material about its structure, microstructure, magnetic and dielectric properties are very important, which are missing in the literature. The main focus of our work is to investigate these preliminary characteristics of BFO/LMO ceramics over wide range of compositions.

In this study, we present an investigation of structure, magnetic characteristics and impedance properties of a solid solution comprising BFO and LMO, wherein the composition was systematically varied. The solid solution combines the FM ordering of LMO and the AFM ordering of BFO materials. We used a few techniques to confirm the phase purity, magnetic properties and impedance behaviour.

II. Experimental

The traditional solid-state reaction method was employed to synthesize powders with following composition xLaMnO$_3$–(1-x)BiFeO$_3$, where x = 0.05, 0.10 and 0.20. The following high-purity raw materials were used in stoichiometric proportions: La_2O_3, Bi_2O_3, Fe_2O_3 and Mn_2O_3 (obtained from Sigma Aldrich, with a purity of 99.9%). The powders were mixed for 1 h using a mortar and pestle. Subsequently, the combined powder was placed in a bottle with zirconia balls and propanol, and subjected to 24 h of ball milling. The resulting dried powder was then calcined at 1200 °C for 12 h in a high-temperature furnace. Following the calcination process, the calcined powder was mixed with 2 wt.% of PVA binder. Pellets with a diameter of 10 mm and thickness of 1 mm were formed from the prepared powder using a hydraulic press with pressure 1000 t/square inch for 5 min. These pellets were then subjected to sintering process at 1400 °C for 2 h. The effect of processing parameters done at preliminary stage of the experiments has driven us to the selected temperature and time period.

XRD data of the sintered samples were collected on Rigaku Miniflex-II in the range of 20° to 80°, with a step size of 0.02° and a speed of 2 °/min with the help of 40 kV and 40 mA supply. The microstructural analysis has been done using field mission scanning electron microscope (FESEM, Plus JEOL 7610F). Magnetic hysteresis loops were obtained at room temperature using a vibrating sample magnetometer (VSM 100, Cryogenic). Furthermore, the impedance spectroscopy (Microtest 6632) was utilized to determine the real (Z') and imaginary (Z'') components of impedance.

III. Results and discussion

3.1. X-ray diffraction

Figure 1 displays XRD spectra of the xLaMnO$_3$–(1-x)BiFeO$_3$ samples, where x = 0.05, 0.10 and 0.20. The crystalline character of the sintered ceramics is confirmed by the sharp and high-intensity peaks. It is well known that there are structural similarities of LMO and BFO compounds with close 2θ values of the characteristic XRD reflections. However, the data from all the samples were precisely correlated with reference card number 98-004-1043 from the EXPERT High Score Software [18]. Theoretical and practical data were very well matched, demonstrating the hexagonal $R\bar{3}c$ symmetry. The fact that all of the peaks match the measured heights shows that the formed solid solutions crystallized into only one phase. Table 1 lists the many parameters that were determined by the Pawley matching. Similar peaks have been observed for all the samples which illustrate the BFO single-phase nature. Moreover, the value of lattice parameters increases which indicates increase in volume. This expansion is due to the presence of larger ions at A (La^{3+} = 1.06 Å and Bi^{3+} = 1.03 Å) and B

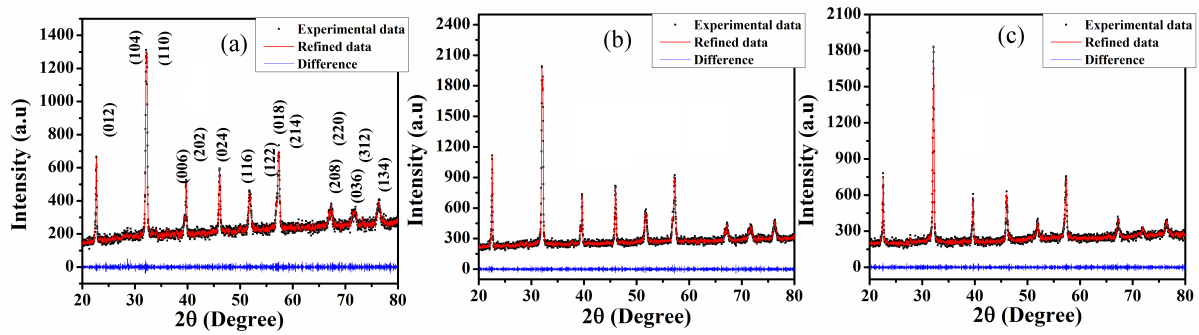

Figure 1. XRD spectra of xLaMnO$_3$–(1-x)BiFeO$_3$ ceramics with different LMO content: a) 0.05, b) 0.10 and c) 0.20

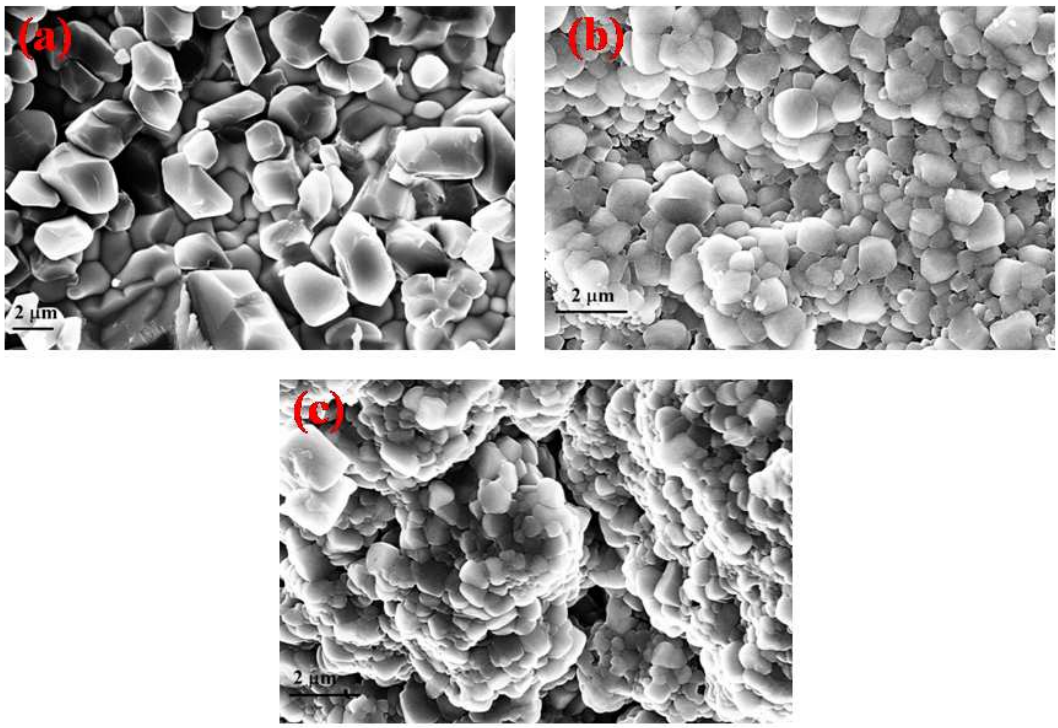

Figure 2. FESEM images of xLaMnO$_3$–(1-x)BiFeO$_3$ ceramics with different LMO content: a) 0.05, b) 0.10 and c) 0.20

(Mn^{3+} = 0.065 Å and Fe^{3+} = 0.064 Å) position as compared to base ions of $BiFeO_3$.

3.2. Microstructure

FESEM micrographs (Fig. 2) clearly show that the grain growth is reduced when the content of LMO increases. This may be due to the doping (i.e. substituting Bi^{3+} with La^{3+} and Fe^{3+} with Mn^{3+}) and the presence of those larger ions at grain boundaries, which hinders the growth of grains. The estimated values of the average grain size and experimental density of the sintered specimens are given in Fig. 3 and Table 1, respectively. It is obvious that xLaMnO$_3$–(1-x)BiFeO$_3$ ceramics with a larger grain size will also have a higher density. Therefore, the addition of LMO slows down the sintering process of BFO ceramics.

3.3. Magnetic property

The magnetization response to an applied magnetic field at room temperature was examined and the results are depicted in Fig. 4. The observed magnetization behaviour of the BFO sample is characteristic of G-type antiferromagnetic (AFM) structures, where neighbouring Fe^{3+} atoms exhibit anti-parallel spin orientations [19]. A very small value of remnant magnetization of 0.037 emu/g was observed for the sample with x = 0.05. It is obvious from Fig. 4 that the antiferromagnetic behaviour of the BFO [19] has changed into weak fer-

Table 1. Parameters obtained from Pawley fitting

Sample - LMO content	a [Å]	c [Å]	c/a	V [Å^3]	Experimental density [g/cm^3]
x = 0.05	5.565	13.857	2.490	429.14	5.85
x = 0.10	5.568	13.861	2.489	429.72	5.80
x = 0.20	5.570	13.872	2.490	430.37	5.67

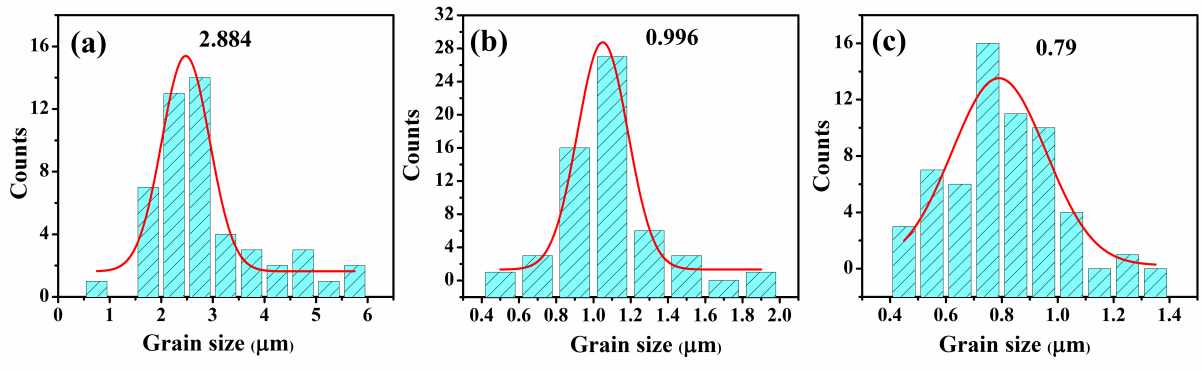

Figure 3. Grain size distribution of xLaMnO$_3$–(1-x)BiFeO$_3$ ceramics with different LMO content: a) 0.05, b) 0.10 and c) 0.20

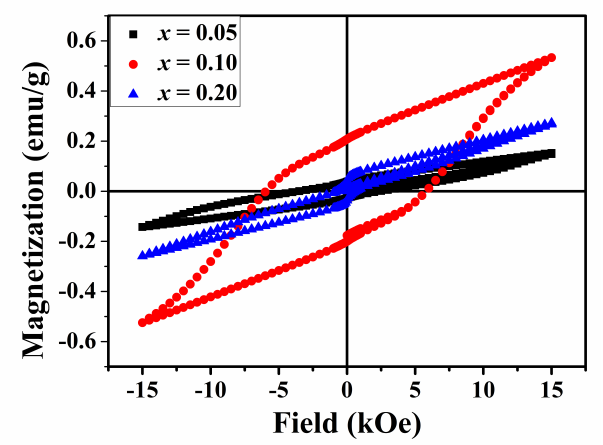

Figure 4. Magnetization versus magnetic field profile for xLaMnO$_3$–(1-x)BiFeO$_3$

romagnetic behaviour in the solid solution containing 5 mol% LMO, with a slight opening of the hysteresis loop and discernible coercivity. The coercive field and remnant magnetization increase with an increase in Mn doping at the Fe position for the sample with x = 0.10. This is probably caused by the contribution of ferromagnetic superposition from LMO which strengthen the superexchange interaction between magnetic ion and oxygen [20–22]. The magnetic dilution of Fe^{3+} ions into Fe^{2+} ions could be an explanation for the decrease in magnetization values caused by further doping [20–22,24]. A magnetic field of 1.5 T does not cause the loop to become saturated. The values of remnant magnetization and maximum magnetization are listed in Table 2.

Table 2. Values of remnant magnetization M_r and maximum magnetization M_s for samples with different LMO content

Sample	M_r [emu/g]	M_s [emu/g]
x = 0.05	0.037	0.157
x = 0.10	0.206	0.533
x = 0.20	0.047	0.274

3.4. Impedance spectroscopy

Figure 5 demonstrates how the real part of impedance (Z') varies with respect to frequency throughout a wide temperature range, i.e. from 50 to 250 °C. The graph shows that Z' exhibits a high magnitude in the lower temperature range and a decreasing trend as frequency rises. The negative temperature coefficient of resistance is characteristic for this kind of behaviour [25,26].

The real part of impedance (Z') decreases as temperature and frequency rise, potentially pointing to an increase in conductivity [27–30]. The reduction in the barrier characteristics of the ceramics is shown by the fact that Z' converges in the high-frequency region in all temperature ranges [27,31]. With an increase in doping concentration from x = 0.05 to 0.20, the value of impedance decreases which in turn leads to an increase in conductivity. This rise in conductivity is clearly due to the increase in the availability of free charge carriers which improves the flow oxygen vacancies created by the mismatch in the ionic size of the parent and doping ions at A and B sites.

Figure 6 shows how the imaginary portion of impedance (Z'') behaves in relation to frequency at var-

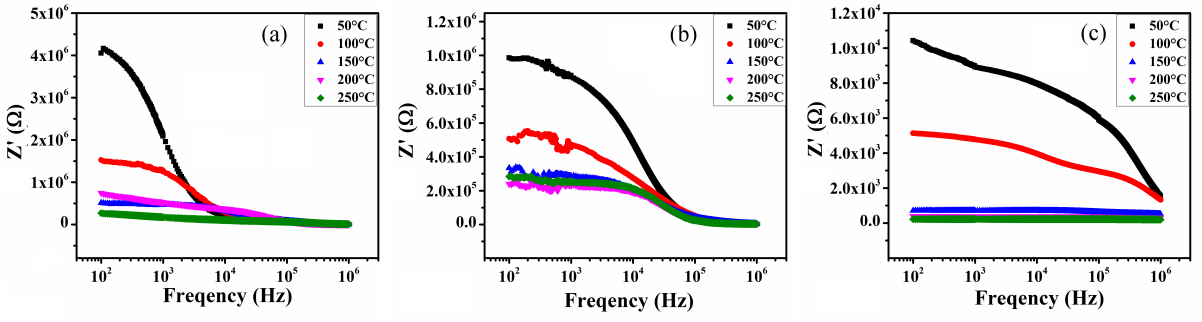

Figure 5. Z' versus frequency of xLaMnO$_3$–(1-x)BiFeO$_3$ ceramics with different LMO content: a) 0.05, b) 0.10 and c) 0.20

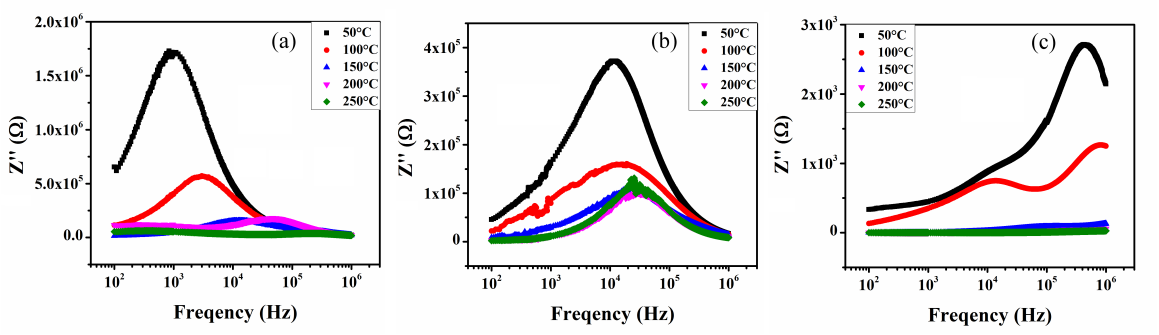

Figure 6. Z'' versus frequency of xLaMnO$_3$–(1-x)BiFeO$_3$ ceramics with different LMO content: a) 0.05, b) 0.10 and c) 0.20

ious temperatures. The trend of Z'' diminishing with temperature and the frequency increase points to a loss of resistive characteristics. The broadening of peaks with rising temperature serves as evidence for the existence of temperature-dependent electrical relaxation processes in the samples. The Z'' curves merge in the high frequency region, indicating that space charge polarization has vanished [26,32]. Additionally, the presence of twin relaxation peaks in Z'' is caused by the coexistence of immobile species at lower temperatures and defect/vacancies at higher temperatures [26,32].

Figure 7 shows the Z'' vs. Z' profile (the Nyquist plots) and frequency domain fitting results at different temperatures ranging from 50 to 250 °C. The presence of a semicircle with its centre below the real axis indicates the non-Debye behaviour, which can be explained by various parameters such as atomic defect distribution, grain orientation, grain boundaries and stress-strain mechanisms [26]. Moreover, the material demonstrates a negative temperature coefficient of resistance (NTCR) behaviour, where the semicircle radius decreases as the temperature rises. Similar behaviour has been found in many researches on BFO and LMO based perovskites. The impedance curves, predominantly influenced by grain and grain boundary conduction, are typically simulated using the Z-VIEW software with a perfect analogue circuit [30,33]. The network consists of several components [34,35], i.e. equivalent circuit in the inset of Fig. 7a. The grain circuit is composed of parallel resistance (R_1) and capacitance (C_1), while the grain boundaries consist of parallel R_2 and C_2 pair. The equation for an equivalent circuit is $Z^* = Z' + iZ''$, where:

$$Z' = \frac{R_1}{1+(\omega_1 R_1 C_1)^2} + \frac{R_2}{1+(\omega_2 R_2 C_2)^2} \quad (1)$$

$$Z'' = \frac{\omega_1 R_1^2 C_1}{1+(\omega_1 R_1 C_1)^2} + \frac{\omega_2 R_2^2 C_2}{1+(\omega_2 R_2 C_2)^2} \quad (2)$$

Here $(\omega_1 R_1 C_1)$ and $(\omega_2 R_2 C_2)$ represent the frequency, resistance and capacitance of the grain and grain boundaries, respectively. While the circular arc sections on the Z axis are used to determine resistance, the following formulas are used to compute capacitance from the maxima of the respective semicircles:

$$C_1 = \frac{1}{\omega_1 R_1} \quad (3)$$

$$C_2 = \frac{1}{\omega_2 R_2} \quad (4)$$

Values of fit parameters for grain (R_1C_1) and grain boundary (R_2C_2) are given in Table 3. R_2 becomes greater than R_1 with increasing temperature, implying that the conducting component in the samples is passing through the grains. Moreover, the excessive linear behaviour for the doped samples having higher doping concentration indicates the lesser contribution of resistance from the grain boundary. The net resistance component is reduced due to the increased number of oxygen vacancies caused by doping concentration.

In comparison with similar systems, we have found that Dy doped BFO shows single relaxation mechanism through bulk grains only [36], and Ca^{2+} doped BFO has very poor impedance of ~1Ω [37]. In the similar temper-

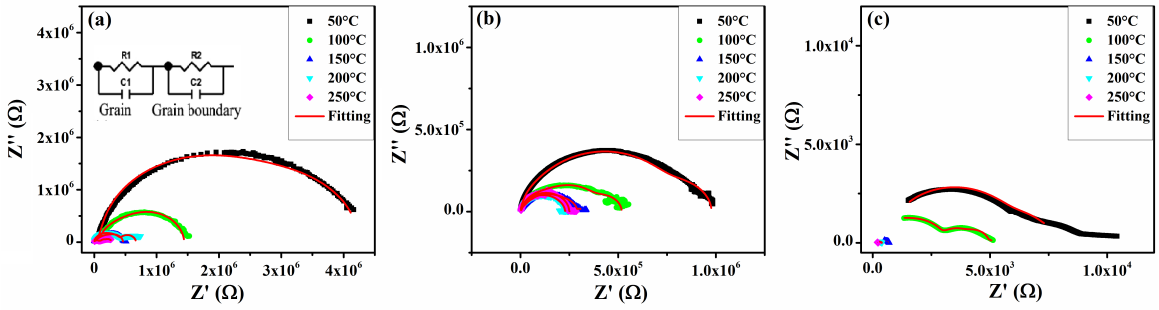

Figure 7. Z'' vs. Z' profile (Nyquist plots) for ceramics with different LMO content: a) 0.05, b) 0.10 and c) 0.20

Table 3. Values of fit parameters for grain (R_1C_1) and grain boundary (R_2C_2)

Temperature	$x = 0.05$				$x = 0.10$				$x = 0.20$			
[°C]	$R_1 \times 10^6$ [Ω]	C_1 [nF]	$R_2 \times 10^6$ [Ω]	C_2 [nF]	$R_1 \times 10^6$ [Ω]	C_1 [nF]	$R_2 \times 10^6$ [Ω]	C_2 [nF]	$R_1 \times 10^6$ [Ω]	C_1 [nF]	$R_2 \times 10^6$ [Ω]	C_2 [nF]
50	2.573	0.012	1.541	0.292	0.129	0.019	0.005	0.057	0.005	0.060	0.000	48.8
100	1.085	0.013	1.801	0.120	0.108	0.021	0.007	0.050	0.005	0.069	0.001	21.9
150	0.343	0.013	2.220	0.077	0.070	0.027	0.174	0.034	0.001	0.071	0.018	10.7
200	0.251	0.035	3.097	0.042	0.029	0.028	0.175	0.029	0.001	0.085	0.023	3.33
250	0.060	0.072	4.032	0.028	0.006	0.043	0.239	0.042	0.001	0.101	0.100	1.9

ature range that we selected, the Ba^{2+} and Gd^{3+} doped BFO have similar trend of impedance values with bulk behaviour only [38]. Moreover, our results show similarity with LMO modified barium titanate in terms of impedance values, but have single semicircle [39]. Furthermore, the Sr substitution in LMO showed little effect on impedance spectra of the base sample in contrast to our case [40].

IV. Conclusions

The solid-state reaction was employed to prepare perovskite xLaMnO$_3$–(1-x)BiFeO$_3$ (x = 0.05, 0.10 and 0.20) powders. The sintered ceramics have single hexagonal phase and grain growth is reduced when the content of LMO increases. The anti-ferromagnetic behaviour of BFO was slowly converted into a ferromagnetic one with the addition of LMO. The value of remnant magnetization increases from 0.037 emu/g for x = 0.05 to 0.206 emu/g for x = 0.10. At various temperatures and frequencies, conductivity values exhibited an upward trend with more doping. All samples had the non-Debye relaxation behaviour, according to impedance spectroscopy. The study established the involvement of grain and grain boundary in conduction phenomenon. With rise in temperature in all the samples, the grain boundary resistance increases which makes conduction through grains possible.

References

1. F. Matsukura, Y. Tokura, H. Ohno, "Control of magnetism by electric fields", *Nat. Nanotechnol.*, **10** (2015) 209–220.
2. S. Dong, J.M. Liu, S.W. Cheong, Z. Ren, "Multiferroic materials and magnetoelectric physics: Symmetry, entanglement, excitation, and topology", *Adv. Phys.*, **64** (2015) 519–626.
3. B.K. Jang, J.H. Lee, K. Chu, P. Sharma, G.Y. Kim, K.T. Ko, K.E. Kim, Y.J. Kim, K. Kang, H.B. Jang, H. Jang, M.H. Jung, K. Song, T.Y. Koo, S.Y. Choi, J. Seidel, Y.H. Jeong, H. Ohldag, J.S. Lee, C.H. Yang, "Electric-field-induced spin disorder-to-order transition near a multiferroic triple phase point", *Nat. Phys.*, **13** (2017) 189–196.
4. J.A. Mundy, C.M. Brooks, M.E. Holtz, J.A. Moyer, H. Das, A.F. Rébola, J.T. Heron, J.D. Clarkson, S.M. Disseler, Z. Liu, A. Farhan, R. Held, R. Hovden, E. Padgett, Q. Mao, H. Paik, R. Misra, L.F. Kourkoutis, E. Arenholz, A. Scholl, J.A. Borchers, W.D. Ratcliff, R. Ramesh, C.J. Fennie, P. Schiffer, D.A. Muller, D.G. Schlom, "Atomically engineered ferroic layers yield a room-temperature magnetoelectric multiferroic", *Nature*, **537** (2016) 523–527.
5. P. Sharma, Y. Heo, B.K. Jang, Y.Y. Liu, J.Y. Li, C.H. Yang, J. Seidel, "Structural and electronic transformation pathways in morphotropic BiFeO$_3$", *Sci. Rep.*, **6** (2016) 32347.
6. P. Mandal, M.J. Pitcher, J. Alaria, H. Niu, P. Borisov, P. Stamenov, J.B. Claridge, M.J. Rosseinsky, "Designing switchable polarization and magnetization at room temperature in an oxide", *Nature*, **525** (2015) 363–366.
7. C. Ji, T. Fan, G.C. A, X. Bai, J. Wang, J. He, W. Cai, R. Gao, X. Deng, Z. Wang, X. Lei, C. Fu, "Influence of sintering method on microstructure, electrical and magnetic properties of BiFeO$_3$-BaTiO$_3$ solid solution ceramics", *Mater. Today Chem.*, **20** (2021) 100419.
8. T. Fan, C. Ji, G. Chen, W. Cai, R. Gao, X. Deng, Z. Wang, C. Fu, "Enhanced the dielectric relaxation characteristics of BaTiO$_3$ ceramic doped by BiFeO$_3$ and synthesized by the microwave sintering method", *Mater. Chem. Phys.*, **250** (2020) 123034.
9. G. Chen, X. Peng, C. Fu, W. Cai, R. Gao, P. Fan, X. Yi, H. Yang, C. Ji, H. Yong, "Effects of sintering method and BiFeO$_3$ dopant on the dielectric and ferroelectric properties of BaTiO$_3$-BiYbO$_3$ based solid solution ceramics", *Ceram. Int.*, **44** (2018) 16880–16889.
10. S. Guan, H. Yang, S. Cheng, Q. Chen, L. Yuan, X. Liu, L. Yang, G. Liu, G. Qiao, "Effects of (Bi$_{0.5}$Li$_{0.5}$)TiO$_3$ addition on microstructures, electrical properties and thermal stability of BiFeO$_3$-BaTiO$_3$ piezoelectric ceramics", *Mater. Sci. Semicond. Process.*, **156** (2023) 107286.
11. H. Ao, H. Wu, W. Li, M. Lan, Z. Zeng, Q. Zhang, R. Gao, X. Deng, G. Chen, C. Fu, Z. Wang, X. Lei, W. Cai, "Effect of sintering temperatures on the magnetoelectric properties of Bi$_{0.78}$La$_{0.08}$Sm$_{0.14}$Fe$_{0.85}$Ti$_{0.15}$O$_3$ ceramics", *Process. Appl. Ceram.*, **16** [2] (2022) 89–96.
12. S. Pillai, D. Bhuwal, A. Banerjee, V. Shelke, "Bulk interface engineering for enhanced magnetization in multiferroic BiFeO$_3$ compounds", *Appl. Phys. Lett.*, **102** [7] (2013) 072907.
13. S. Pillai, D. Tripathi, T. Ahmad Para, A. Das, T. Shripathi, V. Shelke, "Confirmation of enhanced magnetic moment in interface-engineered BiFeO$_3$-LaMnO$_3$ composites", *J. Appl. Phys.*, **120** (2016) 164103.
14. P. Yu, W. Luo, D. Yi, J.X. Zhang, M.D. Rossell, C.H. Yang, L. You, G. Singh-Bhalla, S.Y. Yang, Q. He, Q.M. Ramasse, R. Erni, L.W. Martin, Y.H. Chu, S.T. Pantelides, S.J. Pennycook, R. Ramesh, "Interface control of bulk ferroelectric polarization", *Proc. Nation. Acad. Sci.*, **109** (2012) 9710–9715.
15. D. Yi, J. Liu, S. Okamoto, S. Jagannatha, Y.C. Chen, P. Yu, Y.H. Chu, E. Arenholz, R. Ramesh, "Tuning the competition between ferromagnetism and antiferromagnetism in a

half-doped manganite through magnetoelectric coupling", *Phys. Rev. Lett*., **111** (2013) 127601.
16. H.A. Reshi, A.P. Singh, S. Pillai, R.S. Yadav, S.K. Dhawan, V. Shelke, "Nanostructured $La_{0.7}Sr_{0.3}MnO_3$ compounds for effective electromagnetic interference shielding in the X-band frequency range", *J. Mater. Chem. C*., **3** (2015) 820–827.
17. H.A. Reshi, S. Pillai, R.S. Yadav, T.A. Para, U.P. Deshpande, T. Shripathi, V. Shelke, "Kondo-like electronic transport and ferromagnetic cluster-glass behavior in $La_{0.7}Sr_{0.3}MnO_3$ nanostructures", *RSC Adv*., **5** (2015) 85950–85956.
18. H. Wang, C. Yang, J. Lu, M. Wu, J. Su, K. Li, J. Zhang, G. Li, T. Jin, T. Kamiyama, F. Liao, J. Lin, Y. Wu, "On the structure of α-$BiFeO_3$", *Inorg. Chem.*, **52** [5] (2013) 2388–2392.
19. S. Pillai, H.A. Reshi, T. Bagwaiya, A. Banerjee, V. Shelke, "Enhanced magnetization in morphologically and magnetically distinct $BiFeO_3$ and $La_{0.7}Sr_{0.3}MnO_3$ composites", *J. Appl. Phys*., **122** (2017) 104101.
20. M. Chandra Dimri, H. Khanduri, H. Kooskora, I. Heinmaa, E. Joon, R. Stern, "Magnetic properties and 57Fe NMR studies of U-type hexaferrites", *J. Magn. Magn. Mater*., **323** (2011) 2210–2213.
21. S. Ounnunkad, "Improving magnetic properties of barium hexaferrites by La or Pr substitution", *Solid State Commun*., **138** (2006) 472–475.
22. J. Jia, C. Liu, N. Ma, G. Han, W. Weng, P. Du, "Exchange coupling controlled ferrite with dual magnetic resonance and broad frequency bandwidth in microwave absorption", *Sci. Technol. Adv. Mater*., **14** (2013) 045002.
23. J.J. Xu, C.M. Yang, H.F. Zou, Y.H. Song, G.M. Gao, B.C. An, S.C. Gan, Electromagnetic and microwave absorbing properties of Co_2Z-type hexaferrites doped with La^{3+}", *J. Magn. Magn. Mater*., **321** (2009) 3231–3235.
24. L. Hongying, Z. Haifeng, Y. Lanying, X. Jijing, G. Shucai, M. Jian, H. Guangyan, Preparation and chatactelization of W-type hexafenite doped with La^{3+}", *J. Rare Earths*, **25** (2007) 590–595.
25. T. Badapanda, L.S. Cavalcante, G.E. Da Luz, N.C. Batista, S. Anwar, E. Longo, "Effect of yttrium doping in barium zirconium titanate ceramics: A structural, impedance, modulus spectroscopy study", *Metall. Mater. Trans. A Phys. Metall. Mater. Sci*., **44** (2013) 4296–4309.
26. T. Badapanda, S. Sarangi, B. Behera, S. Anwar, "Structural and impedance spectroscopy study of samarium modified barium zirconium titanate ceramic prepared by mechanochemical route", *Curr. Appl. Phys*., **14** (2014) 1192–1200.
27. S. Mahajan, O.P. Thakur, D.K. Bhattacharya, K. Sreenivas, "Ferroelectric relaxor behaviour and impedance spectroscopy of Bi_2O_3-doped barium zirconium titanate ceramics", *J. Phys. D. Appl. Phys*., **42** (2009) 065413.
28. T. Takenaka, H. Nagata, Y. Hiruma, "Current developments and prospective of lead- free piezoelectric ceramics", *Jpn. J. Appl. Phys.*, **47** (2008) 3787.
29. Priyanka, A.K. Jha, "Electrical characterization of zirconium substituted barium titanate using complex impedance spectroscopy", *Bull. Mater. Sci*., **36** (2013) 135–141.
30. S. Sen, R.N.. Choudhary, "Impedance studies of Sr modified $BaZr_{0.05}Ti_{0.95}O_3$ ceramics", *Mater. Chem. Phys*. **87** (2004) 256–263.
31. A. Kaushal, S.M. Olhero, B. Singh, D.P. Fagg, I. Bdikin, J.M.F. Ferreira, "Impedance analysis of $0.5Ba(Zr_{0.2}Ti_{0.8})O_3$–$0.5(Ba_{0.7}Ca_{0.3})TiO_3$ ceramics consolidated from micro-granules", *Ceram. Int*., **40** (2014) 10593–10600.
32. M.A. Rafiq, M.N. Rafiq, K. Venkata Saravanan, "Dielectric and impedance spectroscopic studies of lead-free barium-calcium-zirconium-titanium oxide ceramics", *Ceram. Int*., **41** (2015) 11436–11444.
33. U. Dash, S. Sahoo, P. Chaudhuri, S.K.S. Parashar, K. Parashar, "Electrical properties of bulk and nano Li_2TiO_3 ceramics: A comparative study", *J. Adv. Ceram*., **3** (2014) 89–97.
34. R. Kaur, V. Sharma, M. Kumar, M. Singh, A. Singh, "Conductivity relaxation in $Pb_{0.9}Sm_{0.10}Zr_{0.405}Ti_{0.495}Fe_{0.10}O_3$ solid solution", *J. Alloys Compd*., **735** (2018) 1472–1479.
35. V. Sharma, R. Kaur, M. Singh, R. Selvamani, S.M. Gupta, V.S. Tiwari, A.K. Karnal, A. Singh, "Conductivity relaxation and oxygen vacancies-related electron hopping mechanism in $Pb_{1-x}La_{x/2}Sm_{x/2}Ti_{1-x}Fe_xO_3$ solid solutions", *J. Asian Ceram. Soc*., **6** (2018) 222–231.
36. L. Thansanga, A. Shukla, N. Kumar, R.N.P. Choudhary, "Study of effect of Dy substitution on structural, dielectric, impedance and magnetic properties of bismuth ferrite", *J. Mater. Sci. Mater. Electron*., **31** (2020) 10006–10017.
37. C.J. Ma, N. Li, W.L. Song, "Tailoring the electrochemical behaviors of bismuth ferrite using Ca ion doping", *Front. Mater*., **7** (2020) 15.
38. R. Das, T. Sarkar, K. Mandal, "Multiferroic properties of Ba^{2+} and Gd^{3+} co-doped bismuth ferrite: Magnetic, ferroelectric and impedance spectroscopic analysis", *J. Phys. D. Appl. Phys*., **45** (2012) 455002.
39. P. Dhak, D. Dhak, M. Das, K. Pramanik, P. Pramanik, "Impedance spectroscopy study of $LaMnO_3$ modified $BaTiO_3$ ceramics", *Mater. Sci. Eng. B*, **164** (2009) 165–171.
40. K. Gupta, O.P. Thakur, M. Kumar, "Effect of A-site substitution on $LaMnO_3$ perovskite via Sr ions for energy applications", *J. Electron. Mater*., **52** (2023) 4279–4288.